NANO LETTERS

Letter

Spinel LiMnO Nanorods as Lithium Ion Battery Cathodes

Do Kyung Kim, P. Muralidharan, Hyun-Wook Lee, Riccardo Ruffo, Yuan Yang, Candace K. Chan, Hailin Peng, Robert A. Huggins, and Yi Cui

Nano Lett., **2008**, 8 (11), 3948-3952 • DOI: 10.1021/nl8024328 • Publication Date (Web): 01 October 2008

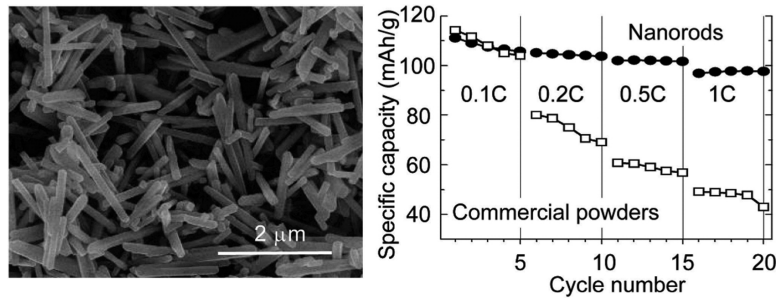

More About This Article

Additional resources and features associated with this article are available within the HTML version:

- Supporting Information
- Access to high resolution figures
- Links to articles and content related to this article
- Copyright permission to reproduce figures and/or text from this article

View the Full Text HTML

Nano Letters is published by the American Chemical Society. 1155 Sixteenth Street N.W., Washington, DC 20036

NANO LETTERS

2008
Vol. 8, No. 11
3948-3952

Spinel $LiMn_2O_4$ Nanorods as Lithium Ion Battery Cathodes

Do Kyung Kim,[†] P. Muralidharan,[†] Hyun-Wook Lee,[†] Riccardo Ruffo,[‡] Yuan Yang,[§] Candace K. Chan,[||] Hailin Peng,[§] Robert A. Huggins,[§] and Yi Cui*[,§]

Department of Materials Science and Engineering, Korea Advanced Institute of Science and Technology (KAIST), Daejeon 305-701, Korea, Dipartimento di Scienza dei Materiali, Università degli Studi di Milano-Bicocca, via Cozzi 53, 20135 Milan, Italy, and Department of Materials Science and Engineering, Department of Chemistry, Stanford University, Stanford, California 94305

Received August 10, 2008

ABSTRACT

Spinel $LiMn_2O_4$ is a low-cost, environmentally friendly, and highly abundant material for Li-ion battery cathodes. Here, we report the hydrothermal synthesis of single-crystalline β-MnO_2 nanorods and their chemical conversion into free-standing single-crystalline $LiMn_2O_4$ nanorods using a simple solid-state reaction. The $LiMn_2O_4$ nanorods have an average diameter of 130 nm and length of 1.2 μm. Galvanostatic battery testing showed that $LiMn_2O_4$ nanorods have a high charge storage capacity at high power rates compared with commercially available powders. More than 85% of the initial charge storage capacity was maintained for over 100 cycles. The structural transformation studies showed that the Li ions intercalated into the cubic phase of the $LiMn_2O_4$ with a small change of lattice parameter, followed by the coexistence of two nearly identical cubic phases in the potential range of 3.5 to 4.3V.

Lithium ion batteries with high energy and power density are important for consumer electronic devices, portable power tools, and vehicle electrification.[1−4] Li_xCoO_2 is a commonly used cathode material in commercial lithium ion batteries and has a charge capacity of 140 mAh/g with a practical value of x from 0.5 to 1. However, the high cost, toxicity, and limited abundance of cobalt have been recognized to be disadvantageous. As a result, alternative cathode materials have attracted much interest. One promising candidate is spinel $LiMn_2O_4$, which has a charge storage capacity of 148 mAh/g.[5−9] Spinel $LiMn_2O_4$ has the advantages of low-cost, environmental friendliness, and high abundance.

Nanostructuring battery electrode materials have been shown to enhance power performance due to the large surface-to-volume ratio that allows for a large electrode−electrolyte contact area.[10−16] Nanowires or nanorods are particularly attractive. Recently we have demonstrated examples of using Si and Ge nanowires as ultrahigh capacity anode materials.[17,18] The nanowire or nanorod morphology not only has a large surface-to-volume ratio but also provides efficient one-dimensional electron transport pathways and facile strain relaxation during battery charge and discharge.

A wide variety of synthetic approaches have been developed for the synthesis of $LiMn_2O_4$ nanoparticles, including combustion,[19,20] sol−gel,[21] solution-phase,[22] and templating[11] methods. Aggregated $LiMn_2O_4$ nanorods have also been produced as cathodes.[23] A facile method is to chemically convert β-MnO_2 nanorods into $LiMn_2O_4$. Here we report the hydrothermal synthesis of single-crystalline β-MnO_2 nanorods and their chemical conversion into free-standing single-crystalline $LiMn_2O_4$ nanorods in a simple solid-state reaction. Battery testing showed that $LiMn_2O_4$ nanorods have a high charge storage capacity at high power operation, which is significantly better than the commercially available powders with particle sizes around 10 μm. More than 85% of the initial charge storage capacity is maintained for over 100 cycles. The structural transformation studies showed that the Li ions intercalated into the cubic phase of the $LiMn_2O_4$ with a small change of lattice parameter, followed by the coexistence of two nearly identical cubic phases in the potential range of 3.5 to 4.3 V.

Experiments. ***Synthesis of MnO_2 and $LiMn_2O_4$ Nanorods.*** Analytical grade $Mn(CH_3COO)_2{\cdot}4H_2O$, $Na_2S_2O_8$ (99.99% Aldrich), and deionized water were used to prepare β-MnO_2 nanorods by hydrothermal reaction as reported elsewhere.[24] All chemicals were used without further purification. In a typical synthesis, $Mn(CH_3COO)_2{\cdot}4H_2O$ and $Na_2S_2O_8$ were dissolved at room temperature with a molar ratio of 1:1 in 80 mL of distilled water by magnetic stirring to form a

* To whom correspondence should be addressed. E-mail: yicui@stanford.edu.
[†] Korea Advanced Institute of Science and Technology (KAIST).
[‡] Università degli Studi di Milano-Bicocca.
[§] Department of Materials Science and Engineering, Stanford University.
[||] Department of Chemistry, Stanford University.

10.1021/nl8024328 CCC: $40.75
Published on Web 10/01/2008

homogeneous clear solution. The mixed solution was transferred to a 100 mL Teflon-lined stainless steel autoclave and heated at 120 °C for 12 h in a preheated electric oven for the hydrothermal reaction. After the reaction, the final precipitated products were washed sequentially with deionized water and ethanol to remove the sulfate ions and other remnants by filtration. The obtained powder was subsequently dried at 100 °C for 12 h in air.

A typical synthesis of $LiMn_2O_4$ nanorods was as follows: 0.00143 moles of $LiOH{\cdot}H_2O$ and 0.0028 moles of the as-synthesized β-MnO_2 nanorods were dispersed into 2 mL high purity ethanol to form a thick slurry, ground to form a fine mixture for several hours, and dried at room temperature. The above process was repeated two to three times to produce a well-mixed powder. The powder was then calcined at 650, 700, and 750 °C in air for 10 h.

The synthesized β-MnO_2 and $LiMn_2O_4$ nanostructures were characterized using an X-ray diffractometer (XRD, Rigaku, D/MAX-IIIC X-ray diffractometer, Tokyo, Japan) with Cu Kα radiation ($\lambda = 0.15406$ nm at 40 kV and 40 mA). The size and shape of the nanostructures were observed on a field emission scanning electron microscope (FE-SEM Philips XL30 FEG, Eindhoven, Netherland), and a high-resolution transmission electron microscope (HR-TEM, JEM 3010, JEOL, Tokyo, Japan).

Electrochemical Investigation. The electrodes for electrochemical studies were prepared by making a slurry of 85 wt % active material of $LiMn_2O_4$, 10 wt % conducting carbon black, and 5 wt % polyvinylidene fluoride (PVDF) binder in *N*-methyl-2-pyrrolidone (NMP) as the solvent. The slurry was applied using a doctor-blade onto an etched aluminum foil current collector and dried at 100 °C for 12 h in an oven. The coated cathode foil was then pressed to form a uniform layer and cut into a square sheet.

The electrochemical performance of the $LiMn_2O_4$ was investigated inside a coffee bag (pouch) cell assembled in an argon-filled glovebox (oxygen and water contents below 2 and 0.1 ppm, respectively). Lithium metal foil (Alfa Aesar) was used as the anode. Typical cathode loading was 1.5 mg/cm^2. A 1 M solution of $LiPF_6$ in ethylene carbonate/diethyl carbonate (EC/DEC, 1:1 v/v) (Ferro Corporation) was used as the electrolyte with a Celgard 2321 triple-layer polypropylene-based membrane as the separator. The charge−discharge cycles were preformed at different C rates between 3.5−4.3 V at room temperature using Bio-Logic VMP3 and Maccor 4300 battery testers. Electrochemical potential spectroscopy was also used to investigate the structural changes in the nanorods. The potential was swept at steps of 3 mV from 3.5 to 4.3 V and vice versa using a cut off current of 8 mA/g.

Result and Discussion. The XRD pattern of the hydrothermal synthesized β-MnO_2 corresponded to JCPDS data No. 24-0735 having tetragonal symmetry with *P*42/*mnm* space group. No additional impurity peaks were detected (Figure 1a). SEM images (Figure 1b) showed that the particles consisted of nanorods with an average diameter of 90 nm and an average length of 1.5 μm.

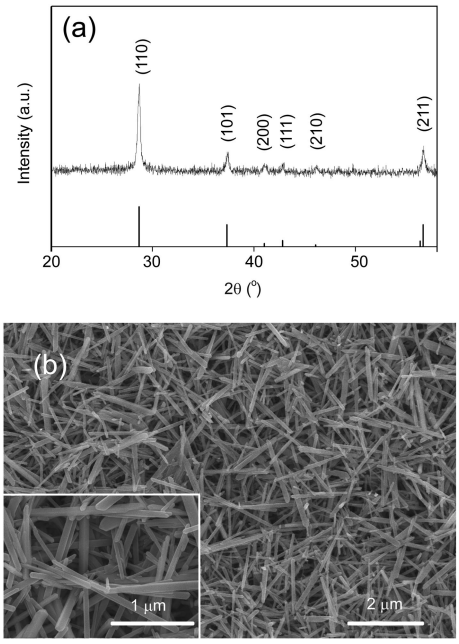

Figure 1. (a) XRD pattern and (b) SEM images of β-MnO_2 as obtained from hydrothermal reaction.

The $LiMn_2O_4$ XRD diffratogram showed features of the spinel structure with *Fd*3*m* space group (JCPS card No. 35-0782), with no peaks of the β-MnO_2 phase detected (Figure 2a). Thus the reaction between β-MnO_2 and LiOH at 700 °C produced the pure $LiMn_2O_4$ phase. To confirm whether the nanorod morphology still remained after the high temperature solid-state reaction, we performed SEM analysis. Figure 2b shows that the $LiMn_2O_4$ phase also consisted mainly of nanorods which appear to have a larger average diameter of 130 nm but a shorter average length of 1.2 μm than the starting β-MnO_2 nanorods. TEM images and diffraction patterns (Figure 2c) show that nanorods are single crystalline and grow along the <110> crystallographic direction.

The electrochemical results are reported in terms of voltage versus lithium concentration (x in $Li_xMn_2O_4$) at constant current (Figure 3a) and voltage versus the differential capacity (dQ/dV) in potentiostatic conditions (Figure 3b) for the first charge and discharge process, as well as cycling properties (Figure 3c,d). During the first charge, at least three electrochemical processes can be observed in the increase of potential (Figure 3a). First, only a small number of charges are stored between the open circuit voltage (around 2.9 V) to 3.8 V, which corresponds to removing the lithium excess from $Li_{1+x}Mn_2O_{4-\delta}$ (around 3.0 V) and removing oxygen vacancies in the lattice (between 3.2 and 3.7 V).[25] Second, at a potential higher than 3.9 V, the material shows the well-known behavior of lithium deintercalation from the $LiMn_2O_4$ cubic spinel phase to the same phase of $Li_{1-x}Mn_2O_4$ (between 3.9 and 4.1 V, delithiation, Figure 3a). Third, a mixture of two cubic phases (plateau around 4.15 V in Figure 3a) is formed until a second single-phase domain of $Li_{0.2}Mn_2O_4$ is reached. The high potential behavior (from 3.9 to 4.2 V) is reversible and two domains (single and two phases) are detected also during the reductive lithiation

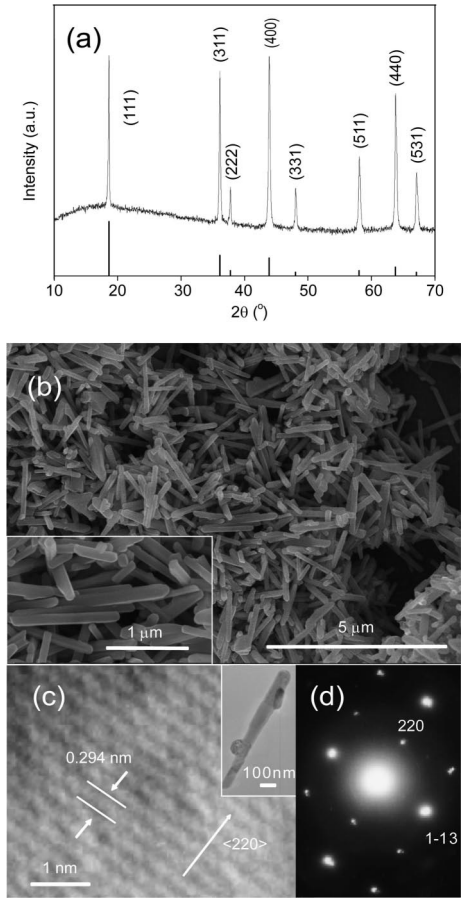

Figure 2. (a) XRD pattern, (b) SEM images, (c) low- and high-resolution TEM of $LiMn_2O_4$ nanorods as obtained from solid-state reaction between β-MnO2 nanorods and $LiOH{\cdot}H_2O$.

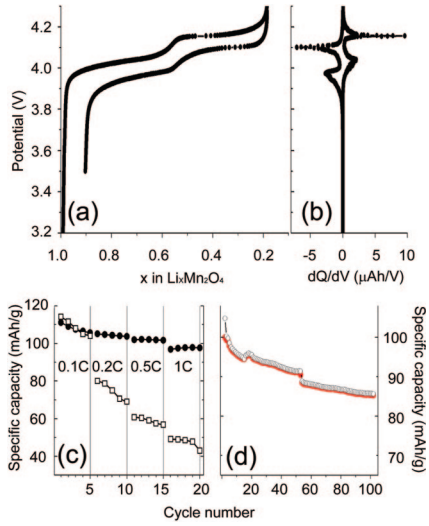

Figure 3. (a) Galvanostatic (0.1 C) first charge/discharge curve, (b) potentiostatic differential capacity vs voltage (dO/dV), (c) discharge specific capacity curve vs number of cycles for nanorods (black dots) and commercial powder electrode (white squares) at different power rates, and (d) charge (white) and discharge (red) specific capacity curve vs number of cycles for nanorod electrode at 1C rate.

(Figure 3b). Moreover very good energy efficiency is observed. In fact, the potential drop between the charge and the discharge process is only 40 mV at the rate of 28.6 mA/g, indicating the fast kinetics of the system. Since we are interested in evaluating the material as the cathode in the Li-ion battery, we used a discharge cutoff value of 3.5 V, which is similar to the requirement for commercial application. At the end of the first discharge the charge excess is lost (Coulombic efficiency of 90%). We have to consider, however, that usually a battery pack is assembled with a certain amount of extra capacity at the cathode to compensate irreversible anode reactions taking place during the first cycle (solid electrolyte interphase (SEI) formation, surface oxide reduction, etc.). In this case, it is an advantage to use the charge excess instead of loading more material at the cathode.

The voltage versus dQ/dV curve clearly points out the different nature of the two processes at high potential (Figure 3b). The former one, at potential ranging from 3.9 to 4.1 V, displays a bell shape peak at 4.05 V which has full width at half-maximum (FWHM) of 55 mV while the latter process shows a spike peak at 4.15 V with just 5 mV in FWHM. The sharp peak observed in this latter peak (Figure 3b) corresponds to a flat plateau in Figure 3a, a clear indication of the coexistence of two phases. The difference between the two processes is also evident during the discharge scan in which they occur at potentials of 4.10 and 3.95 V with FWHM of 10 and 50 mV, respectively.

The discharge specific capacity of the nanorods as a function of cycle number has been compared with the result obtained using an electrode obtained from commercial powders ($LiMn_2O_4$ electrochemical grade, Sigma Aldrich) using the same preparation route (Figure 3c), that is, the commercial electrode is a mixture of active material, carbon black, and binder in the weight ratio of 85:10:5. The charge capacity is measured with the power rate from 0.1 C (14.8 mA/g) to 1 C (148 mA/g). We have observed that the nanorod morphology has a much higher charge capacity than the commercial powders at higher power rates. At the lowest current (from cycle 1 to 5) both the samples have a specific capacity around 110 mAh/g but increasing the rate to 0.2 C (from cycle 6 to 10) leads a large difference in performance: the specific capacity of the nanorod electrode remains almost constant between 110 and 105 mAh/g while that of commercial powder decreases to 70 mAh/g. In most of the literature a larger amount of conductive agent (up to 20%) is added to the active $LiMn_2O_4$ material and the specific discharge capacity obtained at moderate rates such as 0.2 C is comparable to that of our nanorods. However, we point out that in our nanorod case, reducing the amount of carbon black (10 wt %) and increasing the active material ratio means that more charges can be stored in the electrode regardless of the obtained $LiMn_2O_4$ specific capacity. This advantage results from the one-dimensional electron transport and large surface area of the nanorods. The difference of specific charge capacity between the nanorods and commercial powders becomes larger with the further rate increase (Figure 3c). At the highest current (148 mA/g), the nanostructured electrode can deliver a specific charge capacity (100 mAh/g) twice of the commercial powders (50 mAh/g). These data indicate that the large surface-to-volume ratio of the nanorods enhances greatly the kinetics of the $LiMn_2O_4$

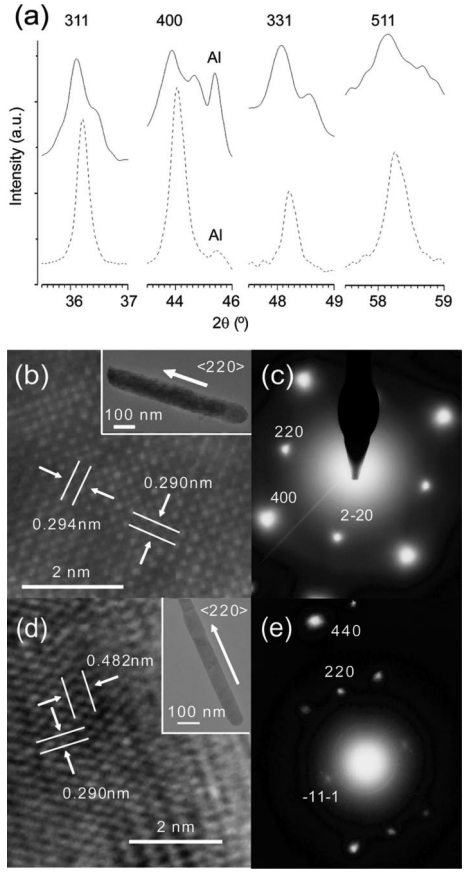

Figure 4. (a) XRD diffraction peaks of $Li_{0.8}Mn_2O_4$ (bottom) and $Li_{0.4}Mn_2O_4$ (top). Al refers to the peak from the Al current collector (b) low and high resolution TEM images of $Li_{0.8}Mn_2O_4$, (c) low and high resolution TEM images of $Li_{0.4}Mn_2O_4$.

electrodes. To evaluate the cyclability of the nanorod electrode at a high rate, we have performed 100 cycles at 1 C. The sample shows very good capacity retention. After 50 and 100 cycles, the capacity retention is 95 and 85%, respectively (Figure 3d). The average Coulombic efficiency is 99.7%. Therefore the $LiMn_2O_4$ nanorods can supply good capacity at high rates with high reversibility.

To better understand the correlation between the structure and the electrochemical behavior of the nanorods, we have exploited XRD and TEM on samples with different lithium amounts. Two electrochemical cells were stopped during the first delithiation charge step (rate 14.8 mA/g, 0.1 C) to obtain compositions of $Li_{0.8}Mn_2O_4$ and $Li_{0.4}Mn_2O_4$, respectively. It was observed (Figure 4a) that the $Li_{0.8}Mn_2O_4$ sample showed an XRD diffraction pattern corresponding to a single crystalline phase having cubic cell parameter of 8.227 Å, which is lower than the pristine $LiMn_2O_4$ (8.243 Å). The decrease of cell parameter with delithiation has already been observed in the literature for cubic spinel.[26] The observed shrinkage of the cell parameter continues until the composition reaches a critical value where a structural change takes place and the potential enters into the two phases domain at ~4.15 V. In fact, the diffraction pattern of $Li_{0.4}Mn_2O_4$ sample appears to be lower in intensity and each reflection clearly splits into two peaks due to the presence of two different cubic phases in this composition domain. Two cubic cell parameters were calculated as 8.24 and 8.17 Å, respectively; therefore the sample should be a mixture of a $Li_xMn_2O_4$ lithium rich and a $Li_yMn_2O_4$ lithium poor compound where x is close to 1.0 and y might be close to 0.2. We also used TEM to compare nanorods with composition of $Li_{0.8}Mn_2O_4$ (Figure 4b) and $Li_{0.4}Mn_2O_4$ (Figure 4c). In both samples, TEM images and electron diffraction showed that nanorods remained single crystalline. However, due to the small difference in cell parameter, the coexistence of the two-phase domains in the $Li_{0.4}Mn_2O_4$ nanorods could not be resolved. The small difference in the two phases should facilitate the fast kinetics of battery charging discharging, consistent with our electrochemical data.

Conclusion. $LiMn_2O_4$ nanorods with cubic spinel structure have been obtained with facile, low-cost and scalable hydrothermal and solid-state reaction methods. The nanorod morphology appears to be a very important step in improving the kinetic properties of the material and the nanorods are able to deliver 100 mAh/g at a high current density of 148 mA/g with high reversibility and good capacity retention after 100 cycles. During the charge step two fundamental processes have been detected and investigated: the delithiation proceeds in a single cubic phase with decreasing of the cubic cell parameter, followed by the coexistence of two cubic phases with similar cell parameters.

Acknowledgment. The work is supported by the Global Climate and Energy Project at Stanford and King Abdullah University of Science and Technology. C.K.C. acknowledges support from a National Science Foundation graduate fellowship and Stanford Graduate Fellowship. D.K.K. would like to thank the SBS Foundation and Korea Research Foundation (KRF-2005-005-JO9701) for supporting his sabbatical leave.

References

(1) Scrosati, B. *Nature* **1995**, *373*, 557.
(2) Chung, S.-Y.; Bloking, J. T.; Chiang, Y.-M. *Nat. Mater.* **2002**, *1*, 123.
(3) Whittingham, M. S. *Chem. Rev.* **2004**, *104*, 4271.
(4) Kang, K.; Meng, Y. S.; Berger, J.; Grey, C. P.; Ceder, G. *Science* **2006**, *311*, 977.
(5) Thackeray, M. M.; Johnson, P. J.; Depicciotto, L. A.; Bruce, P. G.; Goodenough, J. B. *Mater. Res. Bull.* **1984**, *19*, 179.
(6) Thackeray, M. M.; Dekock, A. *J. Solid State Chem.* **1988**, *74*, 414.
(7) Jayalakshmi, M.; Mohan Rao, M.; Scholz, F. *Langmuir* **2003**, *19*, 8403.
(8) Cabana, J.; Valdés-Solís, T.; Palacín, M. R.; Oró-Solé, J.; Fuertes, A.; Marbàn, G.; Fuertes, A. B. *J. Power Sources* **2007**, *166*, 492.
(9) Luo, J.-Y.; Wang, Y.-G.; Xiong, H.-M.; Xia, Y.-Y. *Chem. Mater.* **2007**, *19*, 4791.
(10) Shaju, K. M.; Jiao, F.; Debart, A.; Bruce, P. G. *Phys. Chem. Chem. Phys.* **2007**, *9*, 1837.
(11) Li, N.; Patrissi, C. J.; Che, G.; Martin, C. R. *J. Electrochem. Soc.* **2000**, *147*, 2044.
(12) Belcher, A. M.; Mao, C.; Solis, D. J. U.S. Pat. Appl. WO2005067683-A2, 2005.
(13) Wang, Y.; Cao, G. Z. *Chem. Mater.* **2006**, *18*, 2787.
(14) Li, Y.; Tan, B.; Wu, Y. *Nano Lett.* **2008**, *1*, 265.
(15) Lee, Y. J.; Kim, M. G.; Cho, J. *Nano Lett.* **2008**, *3*, 957.
(16) Arico, A. S.; Bruce, P.; Scrosati, B.; Tarascon, J. M.; Van Schalkwijk, T. *Nat. Mater.* **2005**, *5*, 366.
(17) Chan, C. K.; Peng, H.; Liu, G.; McIlwrath, K.; Zhang, X.-F.; Huggins, R. A.; Cui, Y. *Nat. Nanotechnol.* **2008**, *3*, 31.
(18) Chan, C. K.; Zhang, X. F.; Cui, Y. *Nano Lett.* **2008**, *8*, 307.
(19) Du, K.; Zhang, H. *J. Alloys Compd.* **2003**, *352*, 250.

(20) Kovacheva, D.; Gadjov, H.; Petrov, K.; Mandal, S.; Lazarraga, M. G.; Pascual, L.; Amarilla, J. M.; Rojas, R. M.; Herrero, p.; Rojo, J. M. *J. Mater. Chem.* **2002**, *12*, 1184.
(21) Curtis, C. J.; Wang, J. X.; Schulz, D. L. *J. Electrochem. Soc.* **2004**, *151*, A590.
(22) Nieto, S.; Majumder, S. B.; Katiyar, R. S. *J. Power Sources* **2004**, *136*, 88.
(23) Cho, J. *J. Mater. Chem.* **2008**, *18*, 2257.
(24) Wang, X.; Li, Y. D. *J. Am. Chem. Soc.* **2002**, *124*, 2880.
(25) Gao, y.; Dahn, J. R. *J. Electrochem. Soc.* **1996**, *143* (1), 100.
(26) Ohzuku, T.; Kitagawa, M.; Hirai, T. *J. Electrochem. Soc.* **1990**, *137* (3), 769.

NL8024328